Developmental Biology 450 (2019) 9–22

Contents lists available at ScienceDirect

Developmental Biology

journal homepage: www.elsevier.com/locate/developmentalbiology

Gap junction-dependent coordination of intercellular calcium signalling in the developing appendicularian tunicate *Oikopleura dioica*

Yana Mikhaleva [a], Oleg Tolstenkov [a], Joel C. Glover [a,b,*]

[a] Sars International Centre for Marine Molecular Biology, University of Bergen, Norway
[b] Department of Molecular Medicine, Institute of Basic Medical Sciences, University of Oslo, Norway

ARTICLE INFO

Keywords:
Tunicate
Larvacean
Appendicularian
Connexin
Gap junction
Fertilization
Blastomere
Gastrula
GCaMP6
Calcium channel
Calcium wave
Synchronization
Mibefradil

ABSTRACT

We characterized spontaneous Ca2+ signals in *Oikopleura dioica* embryos from pre-fertilization to gastrula stages following injection of GCaMP6 mRNA into unfertilized eggs. The unfertilized egg exhibited regular, transient elevations in intracellular Ca2+ concentration with an average duration of 4–6 s and an average frequency of about 1 every 2.5 min. Fertilization was accompanied by a longer Ca2+ transient that lasted several minutes. Thereafter, regular Ca2+ transients were reinstated that spread within seconds among blastomeres and gradually increased in duration (by about 50%) and decreased in frequency (by about 20%) by gastrulation. Peak amplitudes also exhibited a dynamic, with a transitory drop occurring at about the 4-cell stage and a subsequent rise. Each peak was preceded by about 15 s by a smaller and shorter Ca2+ increase (about 5% of the main peak amplitude, average duration 3 s), which we term the "minipeak". By gastrulation, Ca2+ transients exhibited a stereotyped initiation site on either side of the 32-64-cell embryo, likely in the nascent muscle precursor cells, and spread thereafter symmetrically in a stereotyped spatial pattern that engaged blastomeres giving rise to all the major tissue lineages. The rapid spread of the transients relative to the intertransient interval created a coordinated wave that, on a coarse time scale, could be considered an approximate synchronization. Treatment with the divalent cations Ni2+ or Cd2+ gradually diminished peak amplitudes, had only moderate effects on wave frequency, but markedly disrupted wave synchronization and normal development. The T-type Ca2+ channel blocker mibefradil similarly disrupted normal development, and eliminated the minipeaks, but did not affect wave synchronization. To assess the role of gap junctions in calcium wave spread and coordination, we first characterized the expression of two *Oikopleura* connexins, Od-CxA and Od-CxB, both of which are expressed during pre-gastrulation and gastrula stages, and then co-injected double-stranded inhibitory RNAs together with CGaMP6 to suppress connexin expression. Connexin mRNA knockdown led to a gradual increase in Ca2+ transient peak width, a decrease of interpeak interval and a marked disruption of wave synchronization. As seen with divalent cations and mibefradil, this desynchronization was accompanied by a disruption of normal development.

1. Introduction

Calcium signaling is an important feature of embryonic development, and has been implicated in events spanning oocyte maturation, fertilization, gastrulation and cell differentiation (Webb and Miller, 2003). Calcium signals during early development have been characterized in several vertebrate and invertebrate species, leading to the discovery of some highly conserved roles, such as in polyspermy block, and also diversity in spatiotemporal patterns, potentially indicative of species-specific intercellular coordination (Stricker, 1999; Webb and Miller, 2003, 2006; Whitaker, 2008). Most studies have focused on a specific developmental time window, and investigations of underlying mechanism have been limited. Combined with the small number of species studied, this provides a motivation to investigate Ca2+ signaling in the embryos of additional species to better address questions of mechanism, overall developmental pattern, and evolutionary conservation and diversity.

Phylogenetically, the tunicate (urochordate) lineage evolved from a common ancestor with the vertebrate lineage, and thus provides a window into the evolutionary origin of vertebrates. Embryonic Ca2+ signaling has been studied previously in only three ascidian tunicate species, *Ciona robusta, Phallusia mammilata* and *Ascidiella aspersa.* In most

* Corresponding author. Sars International Centre for Marine Molecular Biology, University of Bergen, Thormøhlensgt. 55, N-5006, Bergen, Norway.,
E-mail address: joel.glover@medisin.uio.no (J.C. Glover).

https://doi.org/10.1016/j.ydbio.2019.03.006
Received 12 December 2018; Received in revised form 9 March 2019; Accepted 10 March 2019
Available online 21 March 2019

of these studies, the focus was primarily on the Ca2+ transient that arises during fertilization of the egg, and which is involved in preventing polyspermy (Carroll et al., 2003; Stricker, 1999; McDougall and Sardet, 1995; Wilding et al., 2000; Speksnijder et al., 1990; Albrieux et al., 1997). In a recent study, Akahoshi and colleagues used the fluorescent calcium sensor GCaMP6 (a genetically encoded fusion protein of green fluorescent protein, calmodulin, and the M13 peptide sequence from myosin light chain kinase, which responds to Ca2+ binding by emitting fluorescence), to reveal changes in intracellular Ca2+ concentration during gastrulation and larval tissue differentiation in *Ciona robusta and Ciona savignyi* (Akahoshi et al., 2017). They observed Ca2+ transients in multiple tissues including the epidermis, neural tube, heart precursor cells, and tail muscle. They did not assess Ca2+ transients during early cleavage stages nor address experimentally the potential functional role of the Ca2+ transients during development. This prompted us to investigate Ca2+ signaling in the appendicularian tunicate *Oikopleura dioica* using a similar approach employing GCaMP6. Here, we have investigated Ca2+ signaling from pre-fertilization to gastrula stages, longitudinally assessing temporal features and spatial coordination among blastomeres. We manipulated Ca2+ signaling using Ca2+ channel blockers, which disrupted the coordinated spread of Ca2+ transients among blastomeres and led to abnormal development. We thereafter specifically addressed the role of gap junctions in the intercellular coordination of Ca2+ transients by first characterizing the spatiotemporal dynamics of *Oikopleura* connexin expression and then using inhibitory RNA to block connexin expression. This led to an even greater disruption of Ca2+ signal coordination, which again was accompanied by abnormal development.

2. Methods

2.1. Animal culture and handling

Animals were collected in the fjords around Bergen (Norway) and maintained in the new automated *Oikopleura* facility at the Sars Center for several generations before they were used for experiments. Animal culture was as previously described (Bouquet et al., 2009).

2.2. Gene cloning

The following gene-specific primers were designed for connexin CxA (GSOIDT00007538001, GenBank: CBY14509.1) and CxB (GSOIDT00016123001, GenBank: CBY23666.1) genes:

CxA(f1) CGTTGAAGGTGTAATCGTCAAAG
CxA(r1) GATTTTTATGAGCTCGTCGGTTCA
CxA(r2) CTCATCGTCTGTTTTGTAGCTCGG
CxB(f1) TTGTCGGATCAGCTGTTTATGGAG
CxB(f2) GTTTCGCTGCGATACGAATCAGC
CxB(r1) TCGACCGACTGATTTTTTAGTTG
CxB(r2) ATTGACTAACGGCTGGCTCATCTG

Isolation of total RNA from early developmental stages was performed using NucleoSpin® RNA XS (Macherey-Nagel, AH-diagnostics, Oslo, Norway). First strand cDNA synthesis was done with SuperScriptIV Reverse Transcriptase (ThermoFisher Scientific, Oslo, Norway). A PCR was set up with 2 µl of the first strand reaction as template using 0.5 µl of each of the specific primers. The reaction mix consisted of 2.5 µl of 10× NH4+buffer, 1.5 µl of 2.5 mM dNTP, 1.3 µl of 50 mM MgCl2, 0.5 µl of BioTaq enzyme (Bioline, 5U/µl), and 11.5 µl of H2O.

The PCR cycle involved denaturation at 94 °C for 3 min, 35 cycles of 94 °C (15 s each), a 63°C-68 °C gradient (30 s), 68 °C (60 s), followed by elongation at 68 °C for 7 min and storage at 4 °C. PCR products were electrophoresed in a 1% TAE agarose gel. The expected PCR fragment was identified and the gel bands were cut out and purified with QIAquick Gel Extraction Kit (Qiagen, Chatsworth, CA). The PCR fragment was ligated into a pGem-T-Easy Vector system (Promega) in a reaction mixture containing 5 µl of 2× ligation buffer, 1 µl of T4 DNA-ligase, 1 µl of vector (50 ng/µl), and 5 µl of the purified PCR fragment, at 4 °C overnight. Transformation was performed in 20 µl of One Shot™ TOP10 Chemically Competent *E. coli* (ThermoFisher Scientific, Oslo, Norway) with 1 µl of the ligated PCR fragments in the pGEM T-Easy Vector.

The recombinant bacteria were plated out on LB/amp, X-gal, IPTG agar plates and incubated at 37 °C overnight. Two white clones were picked for each primer combination for each gene based on blue-white screening. Colonies were cultured overnight in 5 ml of LB medium (shaking at 37 °C) containing 100 mg/ml ampicillin. Plasmid purification was performed the next day using QIAprep Spin Miniprep Kit (Qiagen). Sequencing reactions were performed for every cloned fragment with BigDye™ Terminator v3.1 Cycle Sequencing Kit (ThermoFisher Scientific, Oslo, Norway) and SP6 and T7 primers.

2.3. Probe synthesis and in situ hybridization

pGemTeasy vector with cloned connexin sequences were used as a template for sense and antisense probe synthesis as described previously (Søviknes and Glover, 2007). Embryos for ISH were collected at different developmental stages (from egg till tailbud) and fixed with 4% paraformaldehyde in 0.5M NaCl in 0.1M MOPS buffer (pH 7.5). In situ hybridization was performed as described previously (Mikhaleva et al., 2015).

2.4. Synthesis of inhibitory dsRNA for CxA and CxB

pGemTeasy vectors with inserts of Connexin1 sequence (CxA(f1)-CxA(r2) – 1021bp) and Connexin2 sequence (CxB(f1)-CxB(r2)- 824bp) were used as templates for PCR amplification with M13(f) and M13(r) primers. Linear DNA fragments of CxA and CxB genes were checked in 1% TAE agarose gels, bands were cut out and purified with QIAquick Gel Extraction Kit (Qiagen, Chatsworth, CA). DNA fragments and L4440 vector were cut with NcoI and SpeI enzymes (NEB) and connexin DNA fragments were ligated into L4440 vector. Transformation was performed into 20 µl of One Shot™ TOP10 Chemically Competent *E. coli* (C404010, ThermoFisher Scientific, Oslo, Norway) using 1.5 µl of the ligated PCR fragments in the L4440 Vector. On the next day two colonies for each gene were picked from agar plates containing 100 mg/ml ampicillin and grown in overnight culture. The plasmids were purified with the Miniprep Kit (Qiagen) in concentration around 250 ng/µl.

1 µl of purified plasmids was used for transformation into 100 µl of homemade HT115 competent cells (Asencio et al., 2003). After dsRNA was generated by the bacterial culture, it was purified as described earlier (Mikhaleva et al., 2015) with the addition of a phenol extraction step to remove protein. The final concentration of dsRNA in the injection mix (ddH2O, mRNA-GCaMP6s) was 900 ng/ml for each of the CxA and CxB genes.

2.5. Quantitative real time PCR (qPCR)

Total RNA was isolated from 25 embryos at early gastrula (n = 3 batches of embryos) and late gastrula (n = 3 batches of embryos) stages of development with NucleoSpin® RNA XS (Macherey-Nagel, AH-diagnostics, Oslo, Norway). sscDNA was generated as described above. RT-qPCR was performed using iQ SYBR Green Supermix (Bio-Rad, Oslo, Norway). Primers for qPCR were designed using the IDT OligoAnalizer 3.1 webtool. An optimal primer pair was chosen for each gene: CxA(f1) - qPCR-CxA(r2) for Connexin1 (147bp expected product), and CxB(f2) - qPCR-CxB(r1) for Connexin2 (111bp expected product). The amplification efficiency was determined by generating a standard curve using serial dilutions of a template and resulted in R2>0.990. The forward primers CxA(f1) and CxB(f2) are shown above in the section "Gene cloning". The reverse primers were the following:

qPCR-CxA(r2) CGCATTTGAAATTTCCGCTTTCGTC

qPCR-CxB(r1) TCGACCGACTGATTTTTTAGTTG.

The BioRAD-qPCR Detection System was used for qPCR. The cycle was: denaturation for 3 min at 95 °C, 39 cycles at 95 °C for 10 s, 65 °C for 30 s and 72 °C for 30 s, with final extension for 30 s at 55 °C, with following temperature increase up to 95 °C. Expression levels of connexin genes were normalized against RPL23–ribosomal protein gene expression. Relative change in mRNA levels between injected and non-injected animals was calculated using the comparative method of relative quantification (Pfaffl, 2001).

2.6. mRNA production

The pSD64-GCaMP6s construct was made based on the pSD64-H2B-EGFP construct (Omotezako et al., 2013), in which the H2B-EGFP sequence was replaced with that of GCaMP6s cDNA (a kind gift from M. Chatzigeorgiou, Sars Center, University of Bergen, Norway). pSD64-GCaMP6s plasmids were linearized with Xba I and used as templates for *in vitro* mRNA transcription with a mMESSAGE mMACHINE SP6 kit (Ambion, Austin, TX). Phenol:chloroform extraction and isopropanol precipitation were used for recovery of the GCaMP6s mRNA. A stock solution of GCaMP6s mRNA [4.7 μg/μl] was stored at −80 °C. mRNA from the stock solution was diluted with water to a working concentration of 0.9–1μg/μl as needed. Working solution of mRNA were stored at −20 °C for up to one month.

2.7. Labeling eggs with Fluo-4

Unfertilized eggs were first treated with *Ciona* dechorionation solution (Kari et al., 2016). 20× inactivated dechorionation solution (20% sodium thioglycolate, 1% pronase in filtered artificial sea water (FASW), 500 μl aliquots stored at −20 °C) was diluted to 1× in 10 ml FASW. 200 μl of 2.5 M NaOH was added to activate the 10 ml 1× dechorionation solution. Eggs were transferred to 1× dechorionation solution for 3 min for permeabilization of the chorion.

Fluo-4AM reagent (Fisher Scientific, Oslo, Norway) was dissolved to 2.5 mM in DMSO and stored at −20 °C as a stock solution. A working solution was freshly made by dilution of 16 μl of stock solution into 8 ml FASW, to a final concentration of 50 μM. Eggs were transferred from *Ciona* dechorionation solution directly into the working Fluo-4AM solution and incubated for 30 min in the dark at 16 °C. After incubation, embryos were washed 2 × 5 min with FASW, and then positioned under the fluorescence microscope for recording of Ca2+ transients.

2.8. mRNA injection and egg fertilization

GCaMP6s mRNA alone or in a mixture with dsRNA-CxA, dsRNA-CxB, dsRNA-CxA/CxB or dsRNA-GAD was injected into unfertilized eggs (Mikhaleva et al., 2018). Injected eggs were transferred to 6-well cell culture plates (VWR, Oslo, Norway), in which the bottoms of the wells were coated with 1% agarose (Promega, Oslo, Norway), and then incubated for 15–20 min in fresh FASW. The 6-well cell culture plate was placed on the observation stage of a Nikon Eclipse TE2000-S inverted microscope for recording of Ca2+ transients, which was initiated prior to fertilization. 50 μl of sperm solution was added to injected and control oocytes some minutes later. Collection of mature animals and preparation of equipment necessary for injections (injection needles, oocyte holding pipettes, FASW and sperm solution) were as described previously (Mikhaleva et al., 2015).

2.9. Imaging and data analysis

Fluorescence measurements were carried out on the Nikon Eclipse TE 2000s inverted microscope outfitted with a 20×/0.45 numerical aperture ELWD (extra long working distance) objective, GFP filter set and 100 W HBO mercury lamp as light source, at 18 °C. 2× binned images were acquired at 250 ms exposure time and 4 frames per second (fps). Image analysis was performed in ImageJ (NIH). Regions of interest (ROIs) were defined to cover either a whole embryo or, for analysis of the temporal spread of Ca2+ signals, 8 divisions of the embryo equally spaced along the anteroposterior axis. Separate ROIs with the same size were selected to measure background fluorescence. Mean intensity values for GCaMP6s or Fluo-4AM fluorescence from each ROI in each video frame were obtained and the difference between this and baseline fluorescence values were normalized to the baseline according to the equation $\Delta F/F_0 = (Fi-F_0)/F_0$, where Fi represents the intensity at a given time point and F_0 represents the average of the baseline fluorescence in 50 frames prior to each transient.

For data analysis, transients were trend corrected by subtracting the linear fitting curve. Peaks were identified as local maxima of the signal above predefined thresholds for peak minima and minimum interpeak intervals. Peak amplitudes, half peak widths and interpeak intervals were measured by built-in MatLab (MathWorks, Natick, Massachusetts, USA) functions.

2.10. Pharmacological manipulation

Stock solutions of the Ca2+ channel blockers nickel dichloride, cadmium dichloride and mibefradil dihydrochloride hydrate (Sigma, Norway) were made at 100 mM in FASW and stored at −20 °C. Working solutions (0.003, 0.03, 0.3 and 3 mM) were made by dilution of stock solutions in FASW. Exposure to blockers was initiated by immediately transferring gastrula stage embryos into working solutions in 6-well cell culture plates. Recording of Ca2+ transients was performed during the first 30 min after exposure. Control embryos were recorded in FASW.

Zero Ca2+ SW was made based on the recipe of Kester et al. (1967). The following amounts of salts were dissolved in 1 L of distilled water: NaCl – 23.9 g, Na2SO4 – 4.0 g, KCl – 0.7 g, NaHCO3 – 0.2 g.

2.11. Statistics

Data are presented as means ± standard deviations. Normality of data was tested by the Shapiro-Wilk normality test, and significance of differences between data set means was determined by the Kruskal Wallis test, Student's *t*-Test or ANOVA (followed by Tukey's post-hoc test) and indicated as p-values (*$p < 0.05$; **$p < 0.01$; ***$p < 0.001$). Data were analyzed and plotted in Excel (Microsoft, USA), in OriginPro (2018) (OriginLab Corporation, Northampton, USA) or in Statistica (TIBCO Software Inc., USA).

3. Results

3.1. Characterization of Ca2+ signals during normal development

3.1.1. Pre-fertilization

Within a few minutes after injecting mRNA encoding GCaMP6 into unfertilized eggs, or of incubating unfertilized eggs in Fluo-4, we could record spontaneous fluorescent signals associated with transient increases in intracellular Ca2+ concentration (Fig. 1). Eggs incubated in Fluo-4, however, soon reduced their Ca2+ activity (Fig. 1B) and did not develop properly, probably as a result of the dechorionation that was required to obtain intracellular loading of the Fluo-4. Each transient began with a small Ca2+ elevation lasting about 3 s, followed by a delay of 10–15 s, after which a much larger elevation of Ca2+ appeared (Fig. 1C). The minor peak (which we hereafter call the "minipeak") was about 5% of the amplitude of the subsequent major peak. This small-large double-peaked waveform is reminiscent of calcium-induced calcium release (CICR), in which an initial influx of Ca2+ through voltage-gated Ca2+ channels triggers release of large amounts of Ca2+ from internal stores (Berridge et al., 2003; Galione et al., 1993) although the latency seen here is much longer than the few 100s of milliseconds that pertains for CICR in neurons, endocrine cells and cardiac muscle cells in

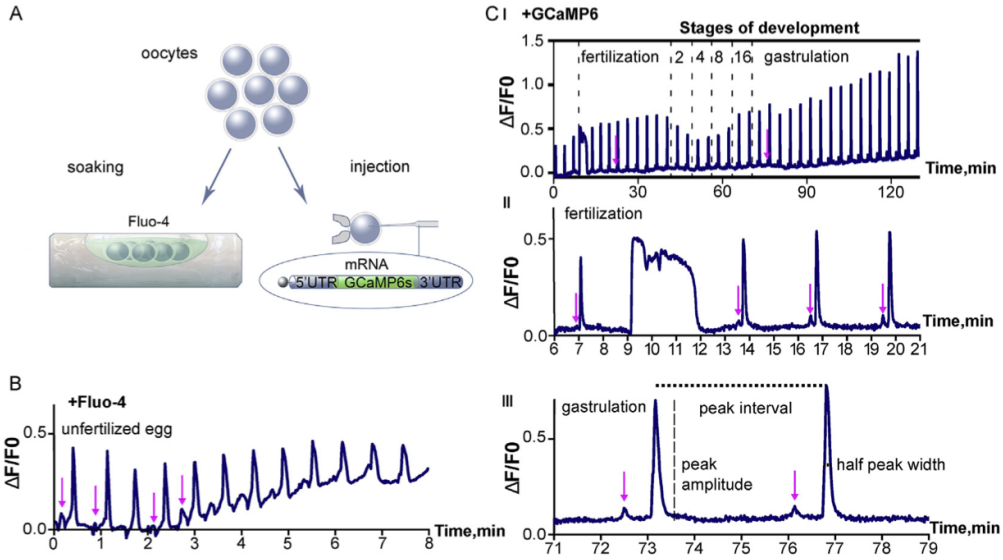

Fig. 1. Spontaneous Ca2+ transients during development of *Oikopleura dioica*. (A) Strategy for labeling unfertilized eggs with Ca2+ sensitive probes for subsequent recording of Ca2+ activity. Left: direct application of Fluo-4 AM dye. Right: injection of GCaMP6s-mRNA. (B) Spontaneous Ca2+ transients in the fertilized egg prior to first cleavage recorded after labeling with Fluo-4 AM dye, measured as the change in fluorescence divided by the baseline fluorescence (delta F/F_0) **Arrows** indicate the Ca2+ minipeaks that precede the main peaks of the transients. (C) Spontaneous Ca2+ transients recorded after injection of GCaMP6s mRNA. (I) Representative sequence of transients from pre-fertilization to gastrula stages, with number of cells at pre-gastrula stages indicated above the transients. (II) Representative sequence of transients before, during and after fertilization at expanded time scale. (III) Two representative transients recorded in the gastrula, with analyzed parameters indicated. In this and subsequent figures, $\Delta F/F_0 = (Fi - F_0)/F_0$, where Fi represents the intensity at a given time point and F_0 represents the average of the baseline fluorescence in 50 frames prior to each transient.

homeothermic species (at around 37 °C (Fabiato, 1983; Verkhratsky, 2002)). The transients were initially weak but gradually increased in amplitude, likely reflecting an ongoing increase in GCaMP6 mRNA translation. Transients were highly regular, with an average half peak width (of the major peak) of 4.2 ± 0.3 s and an average interpeak interval of 2.6 ± 0.4 min (n = 27 eggs). The transients did not arise simultaneously throughout the egg cytoplasm, but typically originated at one side and then spread rapidly (within <2 s) as a wave to the other side, engaging the entire egg volume in the process (Fig. 2; Video S1).

Supplementary video related to this article can be found at https://doi.org/10.1016/j.ydbio.2019.03.006.

3.1.2. *Fertilization*

Due to an evident disturbance of eggs that were dechorionated to permit labeling with Fluo-4AM (they did not exhibit a fertilization-associated Ca2+ transient and did not initiate cleavage), Ca2+ signals associated with fertilization and post-fertilization cleavage stages were only investigated in eggs that had been injected with GCaMP6s mRNA. Fertilization rapidly triggered a much longer lasting Ca2+ elevation with an average duration of 2.25 ± 0.66 min (n = 47 eggs) and an amplitude somewhat greater than the preceding transients in the unfertilized egg. The waveform of the fertilization transient was similar to those described in connection with fertilization in other species, with an initial peak followed by a plateau (Fig. 1DII) (Carroll et al., 2003; Stricker, 1999; Whitaker, 2006). The fertilization Ca2+ transient was initiated at the site of the fertilization cone (equivalent to the site of egg-sperm fusion) and rapidly propagated to the opposite side of the egg. Several minutes later, the polar bodies were visible at the site of Ca2+ transient initiation (Fig. 2A; Video S1).

3.1.3. *Post-fertilization through gastrulation*

Following the fertilization transient, regular spontaneous transients with waveforms (minipeak followed by main peak), half peak widths and interpeak intervals similar to those occurring pre-fertilization were reinstated and continued as cleavage ensued. They were not temporally linked to cleavage events, appearing to follow a separate clock (2.6 ± 0.4 min, n = 27 eggs) relative to the intercleaveage interval, which was 13.2 ± 2.6 min (n = 28 cleavages, n = 8 embryos). Already at the 2-cell stage there was a sequential nature to these transients, as they always originated in one of the blastomeres and then spread to the other, with the blastomeres sometimes switching in the leading role (Fig. 2BC; Video S1). At the 4-cell stage, transients began in one blastomere and quickly spread to the other blastomeres, in one of two patterns: 1) first spreading into the sister blastomere, before spreading from these two sister blastomeres into the neighboring 2 blastomeres (Fig. 2D), or 2) first spreading into the neighboring non-sister blastomere, before spreading from these two blastomeres into their sister blastomeres (Video S1). By the 8-cell stage, it was more difficult to follow transients as they spread among individual blastomeres, but the general impression was that they originated in the two animal blastomeres b (b4.2) and b (b4.2) nearly simultaneously, and then spread to the remaining blastomeres in a coordinated spatial pattern. Here and below we indicate blastomere identity using two different nomenclatures, namely that of Delsman (1910), used by Fujii et al. (2008), and for comparison, in parentheses, that of Conklin (1905), used by Stach et al. (2008). At the 16-cell stage, transients originated in the b2 (b5.3) blastomeres, which give rise to tail muscle cells and epidermal cells, and then spread as a coordinated wave first into neighboring cells and then from the posterior to the anterior pole. This feature was maintained through gastrulation, with Ca2+ wave initiation in the b2 (b5.3) blastomere-derived lineage, and an increasingly complex spatial pattern as the number of cells increased. In the early gastrula, transients originated in the b222 (b7.8) cells, spread symmetrically from these towards the B12 (B6.3) cells (the cells that give rise to tail muscle cells and heart), and from there propagated from posterior to anterior (Fig. 2G; Video S1). This pattern continued as the b222 (b7.8) cells moved to the posterior pole where they become apposed. Ca2+ waves continued to initiate from these and spread from posterior to anterior (Fig. 2H,I,G). At the conclusion of gastrulation, when the invaginating prospective muscle cells migrate over the ventral lip and the lateral sides of the blastopore during tailbud formation, these

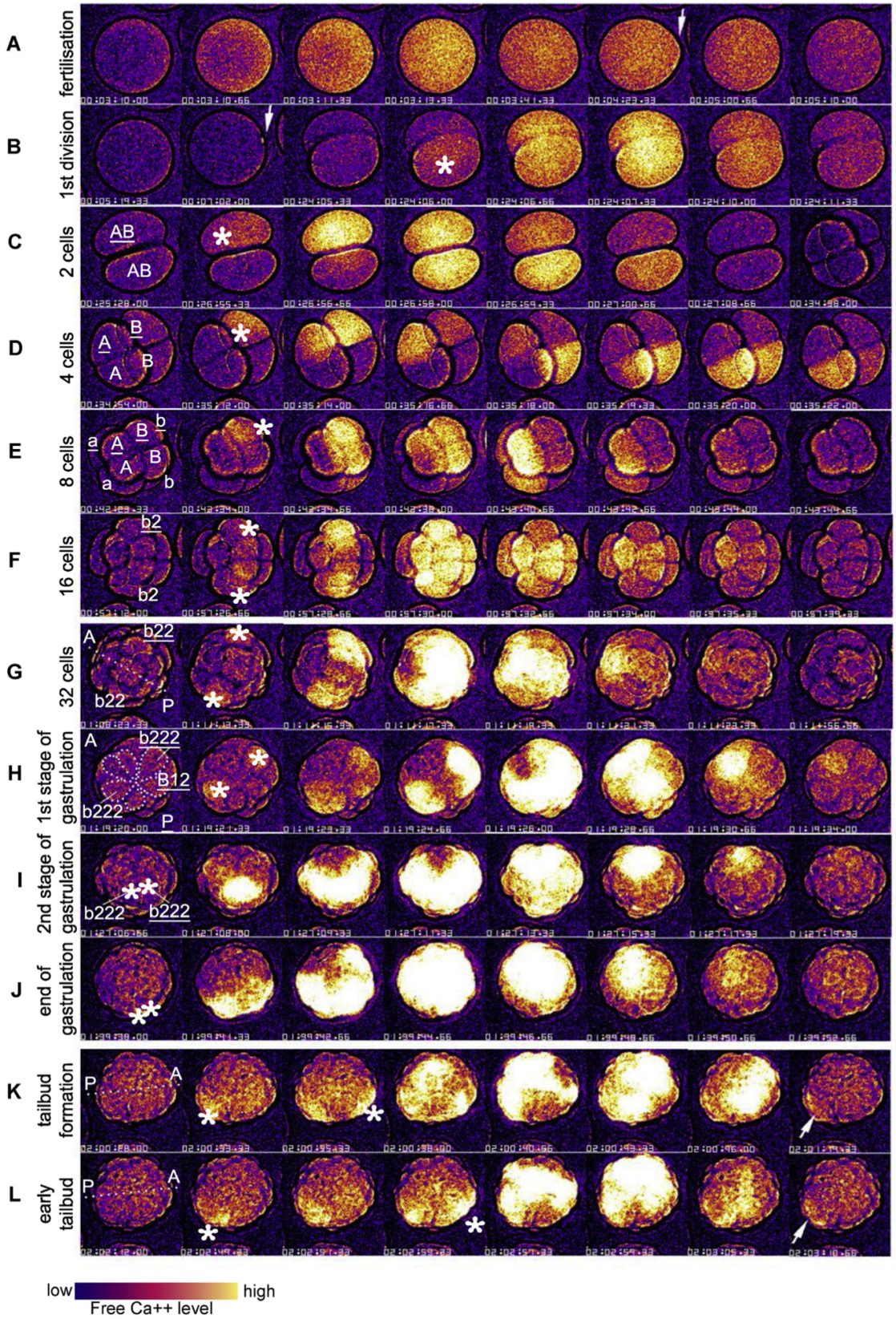

(caption on next page)

Fig. 2. Representative frames from time lapse videos of Ca2+ transients in the developing *Oikopleura* embryo. (A) Fertilization. **Arrow** indicates fertilization cone. (B) Embryo during first cleavage. **Arrow** indicates the polar body, and **asterisk** indicates right blastomere AB, in which the Ca2+ wave was initiated (asterisks in all subsequent panels similarly indicate the origin of the Ca2+ wave). (C) Two-cell stage, anterior to the right. (D) 4-cell stage, anterior to the right. (E) 8-cell stage, viewed from vegetal pole. (F) 16-cell stage, viewed from vegetal pole. **Asterisks** indicate the symmetrically located b2 (animal) blastomeres, in which the Ca2+ wave was initiated. (G) 32-cell stage, viewed from vegetal pole. **Asterisks** indicate the symmetrically located b22 (animal) blastomeres, in which the Ca2+ wave was initiated. A-P indicates the anteroposterior axis. (H) First stage of gastrulation, viewed from vegetal pole. The characteristic "star-like" structure of the cells at the vegetal pole is outlined by the dotted line. **Asterisks** indicate the symmetrically located b222 cells, in which the Ca2+ wave was initiated. (I, J) Second stage of gastrulation. **Asterisks** indicate the b222 cells, which have become apposed. (K) Tailbud formation and (L) tailbud stage, viewed from right side. **Asterisks** indicate cells in which the Ca2+ wave was initiated. **Arrow** indicates tail muscle cells with gradually fading Ca2+ transient. Embryo diameter = 86.4 μm.

cells continued to initiate a Ca2+ wave, but a second initiation site also arose, in what appeared to be prospective trunk epithelial cells. A summary of Ca2+ wave progression at pre-gastrula and gastrula stages (Fig. 3) was made by comparison of video images with published lineage maps (Fujii et al., 2008; Stach et al., 2008).

The main peak amplitudes of post-fertilization Ca2+ transients exhibited a typical temporal dynamic in which the amplitude decreased from the 4-cell to the 16-cell stage and then increased again at about the 32-cell stage. Half peak widths increased gradually by about 50% and interpeak intervals increased by about 20% from the 2-cell to the gastrula stage (Fig. 1CI).

Because half peak widths were always much shorter than the interpeak intervals, the coordinated spread of Ca2+ transients among blastomeres and among gastrula cells represents, on a coarse time scale of minutes, an approximately synchronous event. To simplify description, and as a basis for comparison, in subsequent sections devoted to experimental manipulations we use the term "synchrony" to indicate this closely coordinated wave, in which transients in individual cells occur within a very narrow time window of a few seconds.

Thus, spontaneous, regular Ca2+ transients are initiated already in the unfertilized oocyte and, as the embryo becomes multicellular, evolve into an intercellular Ca2+ wave that spreads through the blastula and gastrula in a stereotyped, coordinated pattern.

3.2. Effects of zero Ca2+ sea water and Ca2+ channel blockers at gastrula stages

Having characterized the temporal and spatial dynamics of the Ca2+ transients, we then attempted to determine whether influx of Ca2+ from the extracellular fluid was involved in initiating them. Since our main interest here was to investigate intercellular Ca2+ waves in the context of the extensive cellular rearrangements that occur during gastrulation (Tada and Concha, 2001; Webb and Miller, 2003), we restricted our experimental manipulations to gastrula stages. Ca2+ transients under experimental conditions were compared to those in control embryos (Video S2). Experimental embryos were transferred to zero Ca2+ sea water, or sea water containing the divalent cations cadmium (Cd2+) or nickel (Ni2+), or the T-type Ca2+ channel blocker mibefradil.

Supplementary video related to this article can be found at https://doi.org/10.1016/j.ydbio.2019.03.006.

3.2.1. Zero Ca2+ sea water

During the time frame analyzed (first 15 min after transfer), exposure of gastrulae to zero Ca2+ sea water did not alter half peak widths, peak amplitudes, the presence of the minipeak or synchronization, but did decrease the interpeak interval from 2.54 ± 0.22 to 1.92 ± 0.29 min (n = 20 embryos) (Figs. 4A,B,C and 5 B, CII; Video S3). By about 20 min after transfer, Ca2+ transients began to drop out (Fig. 4Ai), and further development of the embryo became uncoordinated, such that the structure of most embryos had become disorganized by the gastrula stage and all of them ceased development thereafter (embryos from n = 3 females).

Supplementary video related to this article can be found at https://doi.org/10.1016/j.ydbio.2019.03.006.

3.2.2. Divalent cations

Cd2+ and Ni2+ are typically used to block N-type and T-type voltage-gated Ca2+ channels, respectively, although they also exert intracellular effects (Choong et al., 2014; Permenter et al., 2011). We therefore investigated the effects of these divalent cations as an initial test of a potential role of Ca2+ channels in mediating the Ca2+ transients. Dose-response curves from gastrula to tailbud stages showed that Ni2+ was 10-fold more potent than Cd2+ in disrupting development (Fig. 4D). Both divalent cations, when administered at developmentally disruptive concentrations (0.3 mM for Ni2+ and 3 mM for Cd2+), caused a gradual reduction in major Ca2+ peak amplitude of about 30% for Ni2+ (n = 24 embryos) and 55% for Cd2+ (n = 16 embryos). They also caused a decrease over several cycles of the interpeak interval to 2.15 ± 0.49 min for Ni2+ and 2.21 ± 0.87 min for Cd2+, and an increase of the half peak width from 6.0 ± 1.2 to 10.8 ± 3.6 s for Ni2+ and to 16.8 ± 7.2 s for Cd2+ (Fig. 4A–III,IV, B). Exposure to either cation led to a marked desynchronization (Video S4, Video S5), which was strongest in the case of Cd2+ (Fig. 5B, C-IV,V).

Supplementary video related to this article can be found at https://doi.org/10.1016/j.ydbio.2019.03.006.

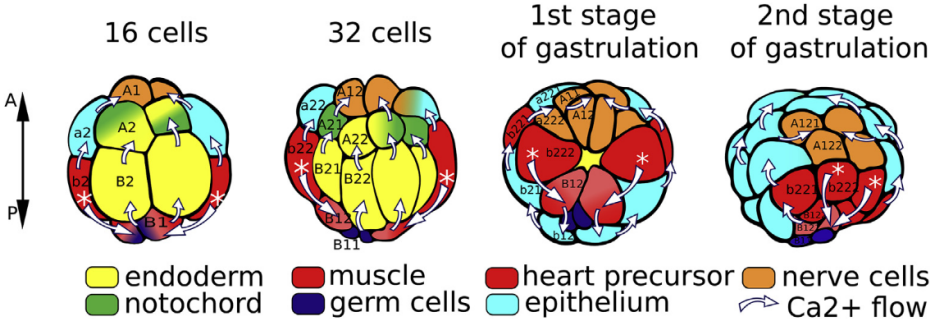

Fig. 3. Schematic diagram of Ca2+ wave propagation at 16-cell, 32-cell and gastrulation stages. Ca2+ transient initiated in the b2 (16-cell stage), b22 (32-cell stage), and b222 (early gastrulation stage) blastomeres, all of which are in the tail muscle cell lineage. See text for details. **Asterisks** indicate blastomeres in which the Ca2+ wave initiates, and **arrows** indicate the trajectory of the Ca2+ wave. **A-P** indicates the anteroposterior axis. Blastomeres of the left side of the embryo are labeled according to the Delsman classification (Delsman, 1910; Fujii et al., 2008). Color code of blastomere derivatives: yellow – endoderm, green – notochord, red – muscle, dark blue – germ line, pink – heart (B12-B121), turquoise – epithelium, orange – nervous system.

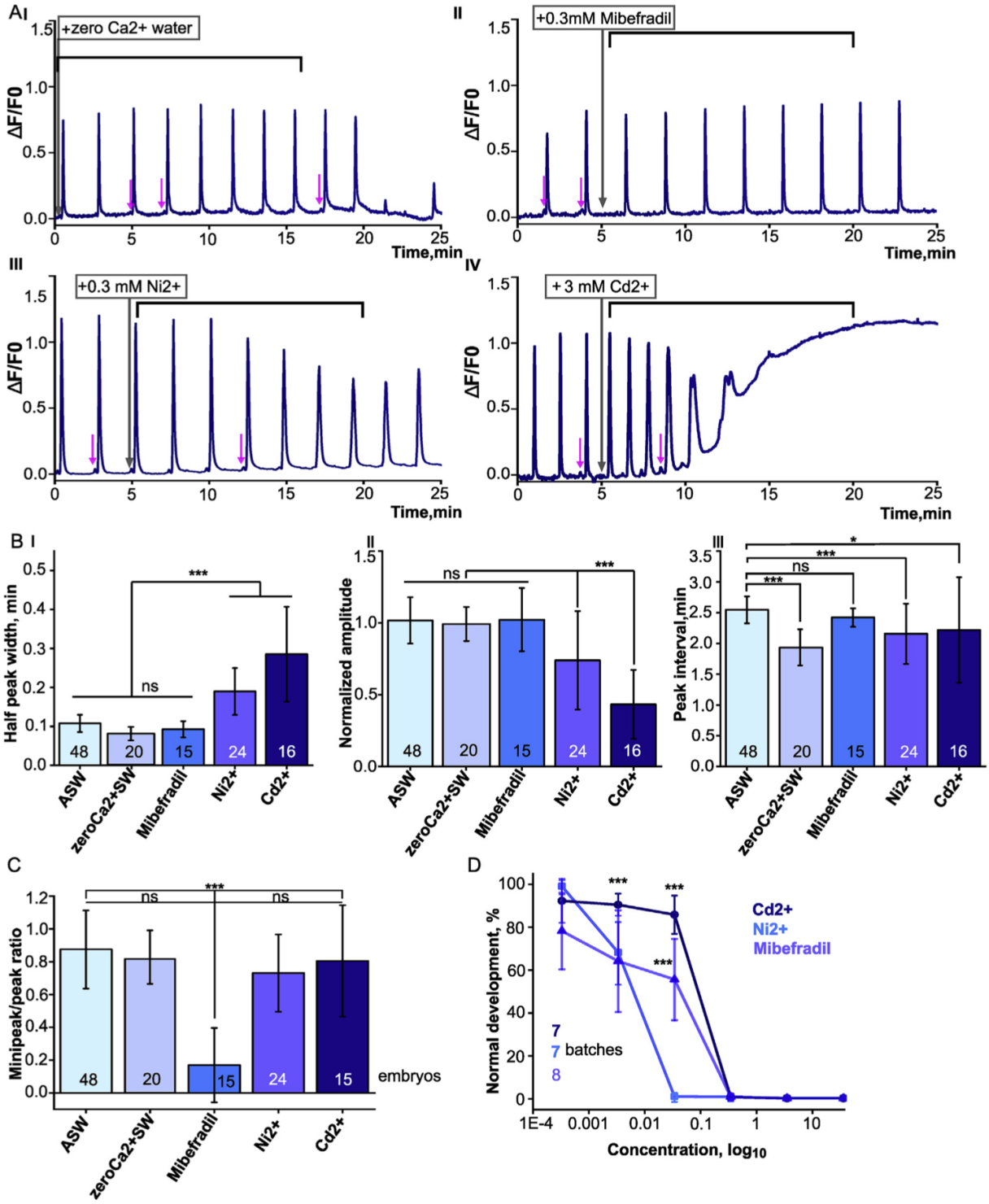

Fig. 4. Effects of zero Ca2+ and Ca2+ channel blockers on Ca2+ transients. (A) Representative Ca2+ transient of embryo treated (I) with zero Ca2+ sea water, (II) with T-type Ca2+ channel blocker mibefradil, (III) with Ni2+, and (IV) with Cd2+. (B) Differences in half peak widths (I), normalized peak amplitudes (II), and interpeak intervals (III). Means ± SDs. (C) Differences in ratio of number of minipeaks to number of major peaks. Means ± SDs. (D) Incidence of normal and abnormal development with and without treatment with divalent cations or mibefradil at different concentrations. P values: * <0.05; ** <0.01; *** <0.001. Timeframe for analysis is indicated in A by brackets. Sample sizes in B and C indicate numbers of embryos, and in D indicate batches of embryos, from each of which ≥25 injected embryos were assessed. Statistical test in B, C and D: ANOVA with Tukey's post hoc test.

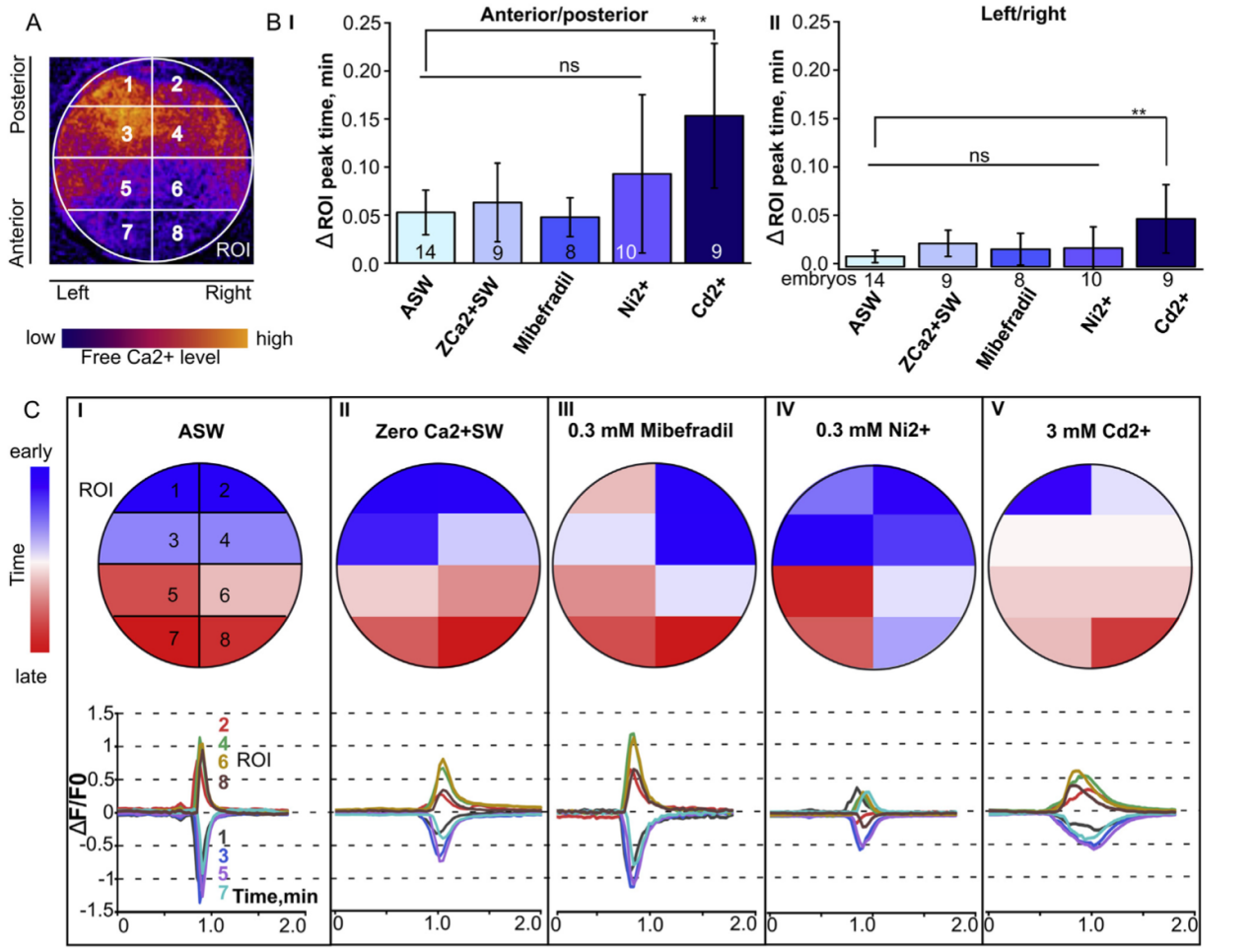

Fig. 5. Effects on propagation of the Ca2+ wave in the gastrula after treatment with zero Ca2+ and Ca2+ channel blockers. (A) Representative image of a gastrula showing the Ca2+ wave in progress. Embryos were divided into 8 ROIs (regions of interest). Peaks were analyzed for each ROI and averaged for 2 Ca2+ waves per embryo, whereafter means and SDs were calculated across embryos. (B) Differences in peak time in ROIs along the anterior-posterior axis (I), and along the left-right axis (II). Means ± SDs. (C) Resulting spatial diagrams indicating time of arrival of transient peaks in the different ROIs (upper panels, color coded according to scale at left) and recorded Ca2+ transient waveforms in each ROI (lower panels, color coded by ROI as indicated, with transients in the left side, odd-numbered ROIs shown as downward deflections in cool colors and transients in the right side, even-numbered ROIs shown as upward deflections in warm colors), for embryos not treated (I) and treated with zero Ca2+ sea water (II), mibefradil (III), Ni2+ (IV) and Cd2+ (V). P values: * <0.05; ** <0.01; *** <0.001. Sample sizes in BI indicate numbers of embryos. Statistical test in B: ANOVA with Tukey's post hoc test.

3.2.3. *T-type Ca2+ channel blocker mibefradil*

The action of divalent cations on Ca2+ channels is not specific to channel type, and it is also difficult to rule out a redistribution of these ions from extracellular to intracellular volumes (Choong et al., 2014; Permenter et al., 2011). We therefore additionally assessed the action of mibefradil, a specific T-type voltage-gated Ca2+ channel blocker (Video S6). The dose-response curve for disrupting development by mibefradil was intermediate between those of Ni2+ and Cd2+. Exposure of gastrulae to developmentally disruptive concentrations of mibefradil did not alter Ca2+ major peak parameters or the synchronization of the Ca2+ wave but significantly reduced (by about 80%) the occurrence of the minipeaks (n = 15 embryos) (Figs. 4AII,B,C and 5B, CIII).

Supplementary video related to this article can be found at https://doi.org/10.1016/j.ydbio.2019.03.006.

We conclude that divalent cations and pharmacological Ca2+ channel blockers impact differently on Ca2+ signaling yet converge on a disruption of normal development at high enough doses. Since they are heterogeneous, we did not pursue the effects of these agents in more detail, but turned our attention instead to experimental manipulations of gap junctions as potential mediators of intercellular Ca2+ signaling.

3.3. *Connexin gene expression*

Connexins belong to the family of integral membrane proteins that when organized into a hexamer comprise a connexon – a half-channel of the gap junction. Each connexin has 4 transmembrane domains (TM) linked by 2 extracellular loops between TM1-TM2 and TM3-TM4 and a cytoplasmic loop (C-loop) between TM2-TM3 (Fig. 6A). They also have N- and C-cytoplasmic ends that exhibit the most variable sequences along with the C-loop. The extracellular loop sequences are more conserved (Abascal and Zardoya, 2013). Each of them includes three cysteins, which generate a cystein bridge through sulfur-sulfur bonds between the connexons of two adjacent cells, thereby forming the intercellular gap junction (Ahir and Pratten, 2014). Gap junctions pass Ca2+ ions, and are integral to the spread of Ca2+ waves among neighboring cells in many tissues (Webb and Miller, 2003).

Around 29 connexin (Cx)-related genes have been found in the *Oikopleura* genome (Denoeud et al., 2010), but only two of them, Od-CxA (GSOIDT00007538001) and Od-CxB (GSOIDT00016123001), appear to be expressed during early cleavage stages according to the OikoBase-gene expression database (Danks et al., 2013) (http://oikoarra

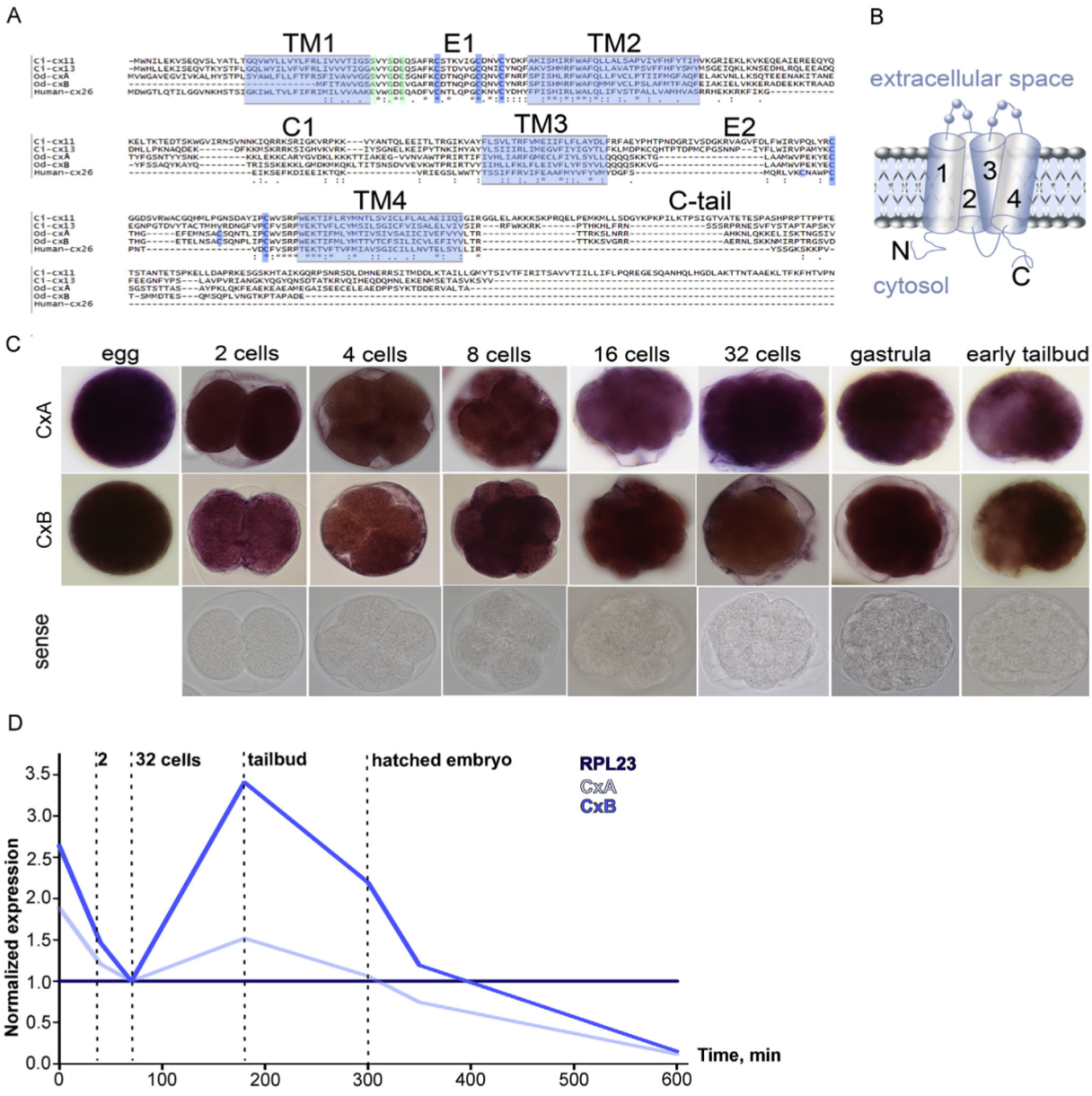

Fig. 6. Sequences, structure and expression of connexin genes Od-CxA and Od-CxB. (A) Amino acid sequence comparison of connexins from *Ciona sp.* (Ci) [Gene model cx-11: KH.C2.1138, cx-13: XP_002131958], *Oikopleura dioica* (Od) [GenBank CxA: CBY14509.1, CxB: CBY23666.1] and human [Pdb_id 1: 5ER7A]. (B) Schematic of the connexin protein with transmembrane domains 1–4 indicated. (C) Results of *in situ* hybridization of Od-CxA and Od-CxB transcripts at the indicated stages. (D) Temporal profile of expression of Od-CxA and Od-CxB normalized to expression of the housekeeping gene RPL23.

ys.biology.uiowa.edu/Oiko/). *Oikopleura* connexin genes exhibited substantial sequence differences from the connexin genes of related tunicates, and of vertebrates (25–30% similarity). For the most conserved region (spanning the TM1-E1-TM2 domains), the percent of amino acid sequence identity increased to about 40–60% with respect to human, mouse, zebrafish and *Ciona* (Table S1).

Comparison of Od-CxA and Od-CxB sequences to the human Cx26 sequence (Bennett et al., 2016) allowed us to recognize all transmembrane domains, and to identify the three conserved cystein residues in the E1–extracellular loop, with positions identical to those in human connexins [C-X6-C-X3-C]. The sequence of the E2–extracellular loop was less conserved. Three cysteine residues were still found [C-X10-C-X7-C] but in a pattern distinct from that in human [C-X4-C-X5-C] (Fig. 6A and B).

We used standard qPCR to quantify Od-CxA and Od-CxB transcripts in the unfertilized egg, at 2- and 32-cell stages and in 5, 7 and 10 h post-hatching larvae. The initial phases of embryonic cleavage occur in the absence of *de novo* transcription and are controlled by maternally inherited mRNAs and proteins (Langley et al., 2014; Tadros and Lipshitz, 2009), up to about the 32-cell stage in the case of Od-connexins. Accordingly, we observed a gradual decrease in Od-CxA and Od-CxB transcript levels up to the 32-cell stage. After this stage, when gastrulation takes place (Fujii et al., 2008; Stach et al., 2008), Od-CxA and Od-CxB transcript levels increased markedly, a likely indication of the maternal-to-zygotic transition (MZT) in connexin transcription. After reaching peaks at the tailbud stage, Od-CxA and Od-CxB transcripts gradually decreased again (Fig. 6D).

In situ hybridization showed that connexin transcripts were expressed

in all cells of the embryo during cleavage and gastrulation until tailbud formation. Thereafter, expression was more specific. Od-CxA transcripts were expressed in all cells except the prospective notochord cells, and Od-CxB transcripts were expressed in all cells except the prospective tail muscle cells (Fig. 6C).

3.4. Effects of connexin mRNA knockdown on embryonic development and Ca2+ transients

3.4.1. Effects on embryonic development

Injection of a mixture of long dsRNA for both Od-CxA and Od-CxB (dsRNA-CxA/CxB) into unfertilized *Oikopleura* oocytes (Fig. 7A) triggered a knockdown of the level of transcripts of both Od-Cx genes, as assessed by qPCR at early and late gastrula stages. Expression of Od-CxA was reduced by five-fold at both stages and expression of Od-CxB was reduced by two-fold at the early gastrula stage and four-fold at the late gastrula stage (Fig. 7B). Similar reductions were obtained after injecting dsRNA-CxA or dsRNA-CxB alone (Fig. S2, n = 3 batches of embryos). In this case the effect of dsRNA-CxA was specific for Od-CxA expression (Fig. S2A), whereas we could not rule out some reduction of Od-CxA expression by dsRNA-CxB (Fig. S2B).

Connexin gene knockdown (of either or both of Od-CxA and Od-CxB) did not affect the development of the embryo through the 32-cell stage, in line with the idea that connexin expression is initially supplied by a maternal stock of transcripts and proteins. However, following injection of dsRNA-CxA/CxB, abnormal development began to manifest during gastrulation, at the time of the MZT. Typically, gastrulation was incomplete and embryonic structure became disorganized, with blastomeres continuing to divide but floundering during ingression and epiboly, the two main processes that implement gastrulation in *Oikopleura* (Fujii et al., 2008; Stach et al., 2008). A less severe abnormal phenotype appeared in some embryos during tailbud formation. In this case gastrulation and tail formation occurred, and sometimes even hatching (Fig. 7C), but the entire process took substantially longer and was accompanied by developmental abnormalities in more than 95% of developing embryos (n = 77 embryos) (Fig. 7C, Video S7, Fig. S1). Less severe developmental disruption also occurred after injection of either dsRNA-CxA or dsRNA-CxB alone, with dsRNA-CxB exerting the least severe effect (Fig. S2C).

Supplementary video related to this article can be found at https://doi.org/10.1016/j.ydbio.2019.03.006.

3.4.2. Effects on Ca2+ transients and Ca2+ wave

In line with the effects on development, injection of dsRNA-CxA/CxB in oocytes affected the temporal parameters of the Ca2+ transients starting at the gastrula stage. The half-peak width increased from 0.16 ± 0.04 to 0.25 ± 0.07 min and the interpeak interval decreased from 3.31 ± 0.22 to 2.19 ± 0.8 min from the early to the late gastrula stage (Fig. 7D and E). The most compelling effect was a prominent disruption of Ca2+ wave synchronization, with a more than 10-fold increase in the time of propagation along anteroposterior and left-right axes (Fig. 7 F, Video S8). Milder effects were seen after injection of either dsRNA-CxA or dsRNA-CxB alone, suggesting that both connexin forms are involved in spread of the Ca2+ wave (Fig. S2, although this conclusion depends on the specificity of each dsRNA for its target connexin RNA). To control for potential non-specific effects of injecting dsRNA *per se*, we injected dsRNA-GAD (targeting transcripts of glutamate dehydrogenase, which is not expressed until the tailbud stage). This had no effect on synchronization of the Ca2+ wave (Fig. 7D).

Supplementary video related to this article can be found at https://doi.org/10.1016/j.ydbio.2019.03.006.

Thus, knockdown of both CxA and CxB mRNA severely disrupts Ca2+ wave propagation and thereby also synchronization.

4. Discussion

In this study, we used Ca2+ imaging to characterize temporal and spatial features of spontaneous Ca2+ transients from pre-fertilization to gastrula stages of the appendicularian tunicate *Oikopleura dioica*. We manipulated Ca2+ signaling using Ca2+ channel blockers and found that this disrupted several features of Ca2+ transients, including (for manipulations of divalent cations, but not exposure to mibefradil) a desynchronization of the Ca2+ wave that normally progresses in a stereotyped, coordinated pattern among blastomeres. We also found that all the Ca2+ channel blockers used also eventually disrupted coordinated development of the embryo. We then characterized the spatiotemporal dynamics of *Oikopleura* connexin expression, and through RNA knockdown explored the role of gap junctions in intercellular Ca2+ signaling. We found that connexin RNA knockdown altered the temporal parameters of Ca2+ transients and led to an even greater degree of Ca2+ wave desynchronization and abnormal development than seen with Ca2+ channel blockers.

Our results indicate that spontaneous, coordinated Ca2+ signaling occurs throughout early embryonic development, starting with regularly timed transients in the unfertilized oocyte and with a gradual evolution of spatiotemporal features as the embryo develops to gastrula and tailbud stages. Disruption of this Ca2+ signaling, either by global pharmacological blockade of Ca2+ channels (and potentially additional intracellular effects of Ca2+ channel blockers) or inhibition of intercellular communication through gap junctions, is accompanied by a disruption of the coordinated cell cleavages and movements that characterize gastrulation and tailbud formation.

4.1. Ca2+ signaling during normal development

Spontaneous Ca2+ signaling during early stages of development has been described in several vertebrate (Chen et al., 2017; Gilland et al., 1999; Tada and Concha, 2001; Webb and Miller, 2003; Whitaker, 2006; Xu et al., 1994) and invertebrate (Kaneuchi et al., 2015; Samuel et al., 2001; Sartain and Wolfner, 2013) species and appears to be a conserved feature that plays an important role in cell-cell communication. Such spontaneous Ca2+ signals are clearly associated with multiple stages of development. Many studies have suggested that spontaneous Ca2+ signaling begins at fertilization (reviewed in Kashir et al., 2013; Stricker, 1999; Webb and Miller, 2007). In some of the species studied, fertilization appears to be required for the initiation of Ca2+ signals (Runft et al., 2002) (Dumollard and Sardet, 2001; Lee et al., 1999). Thus, oocyte activation and fertilization triggers a series of repetitive calcium waves in nemertines (Stricker, 1996), ascidians (Albrieux et al., 1997; Speksnijder et al., 1990), and mammals (Miao et al., 2012; Xu et al., 1994). However, in some cases, for example in teleost fish, eggs can be activated and Ca2+ transients initiated in the absence of sperm by mechanical (Kaneuchi et al., 2015; Sartain and Wolfner, 2013), chemical (Lee et al., 1999) or other stimuli. Here we find that spontaneous, coordinated Ca2+ activity occurs already in the unfertilized oocyte. The trigger for this pre-fertilization activity is unclear, but one possibility is that it might be due to an artifactual stimulation that mimics the triggering effect of fertilization. Both mechanical stimulation associated with the injection of mRNA and enzymatic stimulation associated with the dechorionation required for intracellular loading with Fluo-4 could be involved. Since the pre-fertilization activity had similar characteristics in both GCaMP6s and Fluo-4 AM labeled eggs, impalement of the plasma membrane with an injection micropipette *per se* can be ruled out as a trivial, artifactual explanation. It is worth noting that mechanical stimulation could be involved in connection with the natural spawning event itself, in which eggs are violently discharged from the female gonad, although in this case the chorion is still intact, minimizing mechanical impact directly on the egg plasma membrane.

Of interest is the double-peaked waveform of the spontaneous Ca2+ transients that is observed at all stages. The initial small amplitude

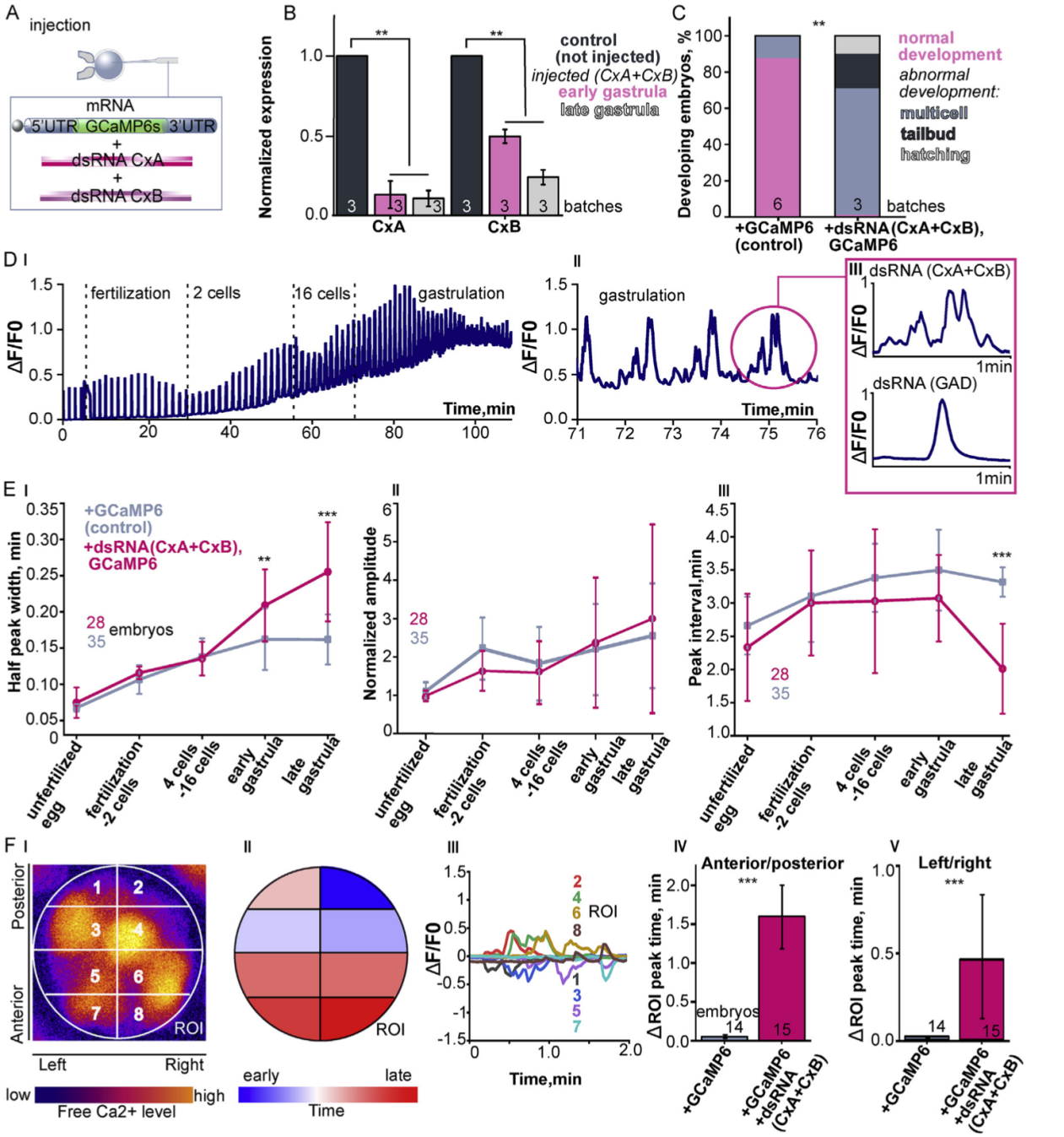

Fig. 7. RNA knockdown of CxA and CxB transcripts disrupts the Ca2+ wave. (A) Schematic illustration of injection of GCaMP6s mRNA and dsRNA-CxA/CxB into an oocyte held fast by a holding suction pipette (to left). (B) qPCR measurement Od-CxA and Od-CxB expression at gastrula stages following injection of dsRNA-CxA/CxB into oocytes. Means ± SDs, normalized to uninjected controls. Sample sizes (n) indicate embryo batches, from each of which 25 injected embryos were collected for analysis. (C) Incidence of normal or abnormal development following injection of dsRNA-CxA/CxB, compared to control (injected with GCaMP6 mRNA). Sample sizes (n) indicate embryo batches, from each of which ≥ 25 injected embryos were collected for analysis. (D) Representative Ca2+ transients after RNA knockdown of both Od-CxA and Od-CxB. (I) Overview spanning from prefertilization to gastrula stages, (II) expanded time scale showing 3 complete transients at gastrula stage, and (III) single transient after injection of dsRNA-CxA/CxB compared to after injection of dsRNA-GAD (control). (E) Effects of dsRNA-CxA/CxB injection on half peak width (I), normalized peak amplitude (II) and interpeak interval (II) at the indicated stages. Means ± SDs. Sample sizes indicate number of embryos. (F) Desynchronized propagation of the Ca2+ wave at the gastrula stage after injection of dsRNA-CxA/CxB. (I) Representative image of the Ca2+ wave with 8 ROIs superimposed, (II) resultant spatial diagram indicating the time at which Ca2+ transients are initiated in the different ROIs, (III) waveforms of the Ca2+ transients in the different ROIs, (IV) effect of dsRNA-CxA/CxB on the difference in transient peak arrival in the first anterior ROI and in the first posterior ROI, as an indication of posterior to anterior propagation, and (V) effect of dsRNA-CxA/CxB on the difference in transient peak arrival in the first left ROI and the first right ROI, as an indication of left-right synchrony. Means ± SDs. P values *< 0.05; **< 0.01; ***< 0.001. Sample sizes in E and F represent number of embryos. Statistical tests in B and C: Kruskal-Wallis; in E: ANOVA with Tukey's post hoc test; in F IV and V: Students t-test.

minipeak followed about 15 s later by the large major peak is reminiscent of calcium-induced calcium release (CICR), which typically involves an initial influx of Ca2+ through voltage-gated Ca2+ channels which then triggers release of large amounts of Ca2+ from internal stores (Berridge et al., 2003; Galione et al., 1993). However, the latency seen here is much longer than in CICR described in other cell types, such as neurons and muscle (Fabiato, 1983; Verkhratsky, 2002). This raises the question of what initiates the initial Ca2+ minipeak in the first place, and how it relates mechanistically to the major peak, which we discuss further in the section on Ca2+ channel blockers below.

The much more protracted fertilization transient arises on the background of the regular spontaneous Ca2+ transients. The waveform of the fertilization transient in *Oikopleura* is similar to that described in connection with the cortical reaction in other species, including other tunicate species, with an initial large peak followed by a plateau (Albrieux et al., 1997; Carroll et al., 2003; McDougall and Sardet, 1995; Speksnijder et al., 1990; Stricker, 1999; Whitaker, 2006; Wilding et al., 2000). Following the termination of the fertilization transient, regular double-peaked spontaneous Ca2+ transients resume with similar timing, suggesting an underlying regular clocklike mechanism that is unaffected by the fertilization transient.

Changing spatial relationships among cells during embryogenesis generates dynamic interactions and potential pathways for pan-embryonic communication by intercellular Ca2+ signalling. This has been suggested to be pivotal in regulating and coordinating the construction of complex three-dimensional embryonic structures (Gilland et al., 1999; Webb and Miller, 2007). In developing *Oikopleura* embryos, intercellular coordination of Ca2+ transients becomes evident at the earliest cleavage stages, and takes on a wave-like appearance by the 16-cell stage. From this stage onwards, there is a highly stereotyped, coordinated pattern of Ca2+ wave propagation. Since the interwave interval (measured in minutes) is much longer than the duration of the transients making up an individual wave (seconds), we have described the wave as a "synchronous" event with a prominent left-right symmetrical pattern. In this context, we have described experimental disruption of the wave as a desynchronization (see below).

Interestingly, in the gastrulae of *Ciona robusta or Ciona savignyi* (Akahoshi et al., 2017; Abdul-Wajid et al., 2015), Ca2+ signals were not reported to be synchronous Ca2+ waves, but rather events arising independently in separate cells. This contrasts with what we have observed in *Oikopleura dioica*, but may be only an apparent difference, due to the lower temporal resolution of recordings made in the earlier studies. More significantly, Ca2+ transients in *Ciona robusta* embryos, when they first occurred (during the late gastrula stage) arose in blastomeres giving rise to the muscle cell lineage (Akahoshi et al., 2017). In another tunicate species, *Boltenia villosa,* voltage-dependent Ca2+ currents were also observed specifically in the muscle lineage blastomeres after gastrulation (Simoncini et al., 1988). We also observed that the initiation of Ca2+ transients occurred in muscle lineage blastomeres in *Oikopleura*, suggesting that this origin is conserved among tunicates. Later, at the stage of tailbud formation, Ca2+ signals in *Oikopleura dioica* become more localized to tissue-specific cell groups (observations which we will elaborate and publish elsewhere). A progressive switch to tissue-specific Ca2+ signaling is reminiscent of the transition from global synchronous waves to localized tissue-specific oscillations seen after gastrulation in zebrafish embryos (Webb and Miller, 2003, 2006, 2007).

4.2. Effects of zero Ca2+ and Ca2+ channel blockers at gastrula stages

One possible mechanism for initiating Ca2+ transients in *Oikopleura* is an influx of extracellular Ca2+ through Ca2+ channels in the plasma membrane. Influx of extracellular calcium can trigger the release of Ca2+ from intracellular stores like the endoplasmic reticulum, which then results in an intracellular wave that propagates throughout the cell cytoplasm (Whitaker, 2008). This sequential pattern is consistent with the double-peaked nature of the observed transients. We therefore tested this idea by changing the extracellular Ca2+ concentration and by blocking voltage-sensitive Ca2+ channels with divalent cations (Ni2+, Cd2+) and the drug mibefradil.

The effect of zero-Ca2+ artificial seawater on various parameters of Ca2+ transients was minimal during the initial 15 min. After about 20 min of exposure, Ca2+ transients began to drop out and development became disrupted. This delayed effect is likely due to the confounding presence of residual Ca2+ in the perivitelline space. Moreover, lowered Ca2+ concentration could influence not only Ca2+ influx, but also cadherin-mediated cell-cell adhesion (Halbleib and Nelson, 2006), a potential cause of the observed developmental disruption. Thus, this manipulation is difficult to interpret.

Ni2+ and Cd2+ are often used to block T-type voltage-sensitive Ca2+ channels, but also exert a number of intracellular effects (Choong et al., 2014; Permenter et al., 2011). Many studies in diverse cellular systems have shown that exposure to the concentrations of Ni2+ and Cd2+ we used here induces an increase in cytoplasmic Ca2+ concentration and defective homeostatic restoration of Ca2+ levels (Choong et al., 2014; Lacinova, 2011; Ruta et al., 2014). Exposure of *Oikopleura* gastrulae to Ni2+ and Cd2+ altered the spatiotemporal parameters of Ca2+ transients, but to different degrees and with some qualitative differences. Both decreased major peak amplitudes and increased peak half-widths substantially without affecting interpeak intervals or the correlation of minipeak and major peak occurrence, but Cd2+ also induced a gradual and marked rise in baseline Ca2+ concentration. Exposure to either cation disrupted Ca2+ wave synchronization and also development. The effects of Ni2+ and Cd2+ on Ca2+ transients and waves are more complex than expected from a simple block of Ca2+ influx through voltage-sensitive Ca2+ channels in the plasma membrane. This is consistent with additional intracellular effects (Choong et al., 2014; Permenter et al., 2011), which may have occurred since we cannot rule out a redistribution between extracellular and intracellular compartments over time. These experimental manipulations thus support the idea that Ca2+ influx through Ca2+ channels in the plasma membrane may be involved, and also indicate that normal Ca2+ signaling is required for normal development, but they are likely confounded by multiple sites of action.

Mebifradil blocks T-type Ca2+ channels much more strongly than other types of voltage-dependent Ca2+ channels, and is commonly used as a selective T-type channel blocker (Leuranguer et al., 2001; Martin et al., 2000). Incubation in 0.3 mM mibefradil eliminated the initial Ca2+ minipeak, but affected other Ca2+ transient parameters only moderately (aside from decreasing peak half-width). This result is consistent with the idea that the Ca2+ minipeak is due to influx of Ca2+ through T-type Ca2+ channels in the plasma membrane, but not the idea that this influx triggers subsequent release from intracellular stores, as couched in the general concept of calcium-induced calcium release (CICR) (Berridge et al., 2003; Galione et al., 1993). This indicates either that the initial minipeak, and potentially Ca2+ influx through the plasma membrane, is not required for regular initiation of Ca2+ transients in *Oikopleura*, or alternatively, that a much smaller minipeak still occurs in the presence of mibefradil, but goes undetected by GCaMP6s imaging yet is still sufficient to trigger the major peaks. Irrespective of its relative effects on minipeaks and major peaks, mibefradil disrupted development (like Ni2+ and Cd2+), but did not affect Ca2+ wave synchronization (unlike Ni2+ and Cd2+). A similar result has been seen in oocytes of the ascidian *Styela plicata,* in which mibefradil treatment significantly reduced Ca2+ current amplitude (measured electrophysiologically) and induced a significant reduction in cleavage rate and disrupted larval development (Gallo et al., 2013).

Thus, calcium channel blockers exert a number of expected effects based on earlier studies, but the complexity of calcium signaling precludes us from achieving a mechanistic understanding of the events underlying spontaneous Ca2+ transients in *Oikopleura* based only on the experiments we have performed here. A much more comprehensive investigation will be needed to dissect out the mechanisms involved.

4.3. Role of gap junctions in intercellular Ca2+ wave propagation

Coordination of intercellular Ca2+ waves at multicellular embryonic stages is presumably mediated by intercellular communication. Intracellular Ca2+ elevation can mobilize intracellular inositol-1,4,5-trisphosphate (IP3) stores or induce exocytotic release of ATP, or both. Both Ca2+ and IP3 can diffuse into adjacent cells through gap junctions (Boitano et al., 1992; Levin, 2007; Robb-Gaspers and Thomas, 1995) and can thus propagate Ca2+ waves across a population of interconnected cells (Webb and Miller, 2003). Alternatively, ATP released into the extracellular space can activate adjacent cells through purinergic receptors, which in turn can stimulate intracellular Ca2+ elevation and thus mediate intercellular propagation of the Ca2+ wave (Jørgensen et al., 1997). Particularly interesting in this regard is the indication that gradients of both Ca2+ and IP3 help establish the dorsoventral (D–V) axis in the developing embryos of diverse animal species (Ault et al., 1996; Jaffe, 1999; Levin, 2007).

We tested specifically the role of gap junctions in Ca2+ wave propagation through connexin RNA knockdown. This provided clear evidence that gap junctions are indeed important for the intercellular communication underlying coordinated Ca2+ signaling in *Oikopleura*. Inhibiting Od-CxA and Od-CxB transcripts markedly disrupts left-right and anteroposterior synchronization of the intercellular Ca2+ wave. The desynchronization is not due to a non-specific effect of injecting dsRNA *per se*, since it was not seen after injection of dsRNA-GAD. It also occurs despite what is obviously incomplete knockdown of Od-CxA and Od-CxB transcripts. It would be interesting to see how a complete knockdown or knockout of connexin expression impacted on Ca2+ wave propagation, although accomplishing this might have additional deleterious effects beyond Ca2+ signaling.

4.4. Future perspectives

Our focus here has been primarily on the characterization of Ca2+ signaling dynamics in the early *Oikopleura* embryo and the role of gap junctions in the intercellular transmission of these signals. More comprehensive mechanistic studies will be needed to 1) tease apart the role of extracellular and intracellular Ca2+, and the roles of associated intracellular signaling pathways, in generating these signals and 2) understand the site-specific initiation and regular timing of the spontaneous Ca2+ transients. This represents a major endeavor for which the present study provides a springboard.

Our current efforts are in a different direction. Normal organogenesis involves diverse morphogenetic processes in which Ca2+ signaling has been implicated. Ca2+ plays well known roles in the development of the nervous system, kidney, heart and muscle (Ahir and Pratten, 2014; Webb and Miller, 2003; Yancey et al., 1992). We have briefly noted here that apparently tissue-specific Ca2+ transients become recognizable during tailbud formation in *Oikopleura*. We intend to investigate tissue-specific Ca2+ signals during late embryogenesis in more detail. Many other *Oikopleura* connexin genes start to be expressed during tailbud formation and are likely to have tissue-specific and stage-specific expression patterns. This motivates a detailed description of connexin gene expression patterns as they relate to Ca2+ signaling in different tissues, paired with selective experimental manipulation of the various connexins through mRNA knockdown. An exciting aspect in this regard involves Ca2+-dependent gene activation. Correlating tissue-specific Ca2+ signaling with the expression of relevant transcription factors should shed light on the role of Ca2+ signaling in tissue specification and the emergence of different organ systems. This will also provide another comparative facet to an evolutionary view of Ca2+ signaling in chordate development.

Funding

This work was funded by the Norwegian Research Council.

Acknowledgements

We thank the Sars Center Appendicularia Facility for supplying the *Oikopleura* specimens used in this study, and Daniel Chourrout and Nick Spitzer for critical evaluation of the manuscript.

Appendix A. Supplementary data

Supplementary data to this article can be found online at https://doi.org/10.1016/j.ydbio.2019.03.006.

References

Abascal, F., Zardoya, R., 2013. Evolutionary analyses of gap junction protein families. Biochim. Biophys. Acta Biomembr. 1828, 4–14.
Abdul-Wajid, S., Morales-Diaz, H., Khairallah, S.M., Smith, W.C., 2015. T-type calcium channel regulation of neural tube closure and EphrinA/EPHA expression. Cell Rep. 13, 829–839.
Ahir, B.K., Pratten, M.K., 2014. Structure and function of gap junction proteins: role of gap junction proteins in embryonic heart development. Int. J. Dev. Biol. 58, 649–662.
Akahoshi, T., Hotta, K., Oka, K., 2017. Characterization of calcium transients during early embryogenesis in ascidians Ciona robusta (Ciona intestinalis type A) and Ciona savignyi. Dev. Biol. 431, 205–214.
Albrieux, M., Sardet, C., Villaz, M., 1997. The two intracellular Ca2+release channels, ryanodine receptor and inositol 1,4,5-trisphosphate receptor, play different roles during fertilization in ascidians. Dev. Biol. 189, 174–185.
Asencio, C., Rodríguez-Aguilera, J.C., Ruiz-Ferrer, M., Vela, J., Navas, P., 2003. Silencing of ubiquinone biosynthesis genes extends life span in Caenorhabditis elegans. FASEB J. 17, 1135–1137.
Ault, K.T., Durmowicz, G., Galione, A., Harger, P.L., Busa, W.B., 1996. Modulation of Xenopus embryo mesoderm-specific gene expression and dorsoanterior patterning by receptors that activate the phosphatidylinositol cycle signal transduction pathway. Development 122, 2033–2041.
Bennett, B.C., Purdy, M.D., Baker, K.A., Acharya, C., McIntire, W.E., Stevens, R.C., Yeager, M., 2016. An electrostatic mechanism for Ca 2+-mediated regulation of gap junction channels. Nat. Commun. 7, 8770.
Berridge, M.J., Bootman, M.D., Roderick, H.L., 2003. Calcium signalling: dynamics, homeostasis and remodelling. Nat. Rev. Mol. Cell Biol. 4, 517–529.
Boitano, S., Dirksen, E.R., Sanderson, M., 1992. Intercellular propagation of calcium waves mediated by inositol trisphosphate. Science 258, 292–295, 80.
Bouquet, J.M., Spriet, E., Troedsson, C., Ottera, H., Chourrout, D., Thompson, E.M., 2009. Culture optimization for the emergent zooplanktonic model organism Oikopleura dioica. J. Plankton Res. 31, 359–370.
Carroll, M., Levasseur, M., Wood, C., Whitaker, M., Jones, K.T., McDougall, A., 2003. Exploring the mechanism of action of the sperm-triggered calcium-wave pacemaker in ascidian zygotes. J. Cell Sci. 116, 4997–5004.
Chen, J., Xia, L., Bruchas, M.R., Solnica-Krezel, L., 2017. Imaging early embryonic calcium activity with GCaMP6s transgenic zebrafish. Dev. Biol. 430, 385–396.
Choong, G., Liu, Y., Templeton, D.M., 2014. Interplay of calcium and cadmium in mediating cadmium toxicity. Chem. Biol. Interact. 211, 54–65.
Conklin, E.G., 1905. Organization and cell lineage of the ascidian egg. J. Acad. Nat. Sci. Phila. 13 (2), 1–119 plates I-XII.
Danks, G., Campsteijn, C., Parida, M., Butcher, S., Doddapaneni, H., Fu, B., Petrin, R., Metpally, R., Lenhard, B., Wincker, P., et al., 2013. OikoBase: a genomics and developmental transcriptomics resource for the urochordate Oikopleura dioica. Nucleic Acids Res. 41, 845–853.
Delsman, H.C., 1910. Beitrage zur Entwicklungsgeschichte von Oikopleura dioica. Verh. Rijksinst. Onderz. Zee. 3, 3–24.
Denoeud, F., Henriet, S., Mungpakdee, S., Aury, J.-M., Da Silva, C., Brinkmann, H., Mikhaleva, Y., Olsen, L.C., Jubin, C., Cañestro, C., et al., 2010. Plasticity of animal genome architecture unmasked by rapid evolution of a pelagic tunicate. Science 330, 1381–1385, 80.
Dumollard, R., Sardet, C., 2001. Three different calcium wave pacemakers in ascidian eggs. J. Cell Sci. 114, 2471–2481.
Fabiato, A., 1983. Calcium-induced release of calcium from the cardiac sarcoplasmic reticulum. Am. J. Physiol. Physiol. 245, C1–C14.
Fujii, S., Nishio, T., Nishida, H., 2008. Cleavage pattern, gastrulation, and neurulation in the appendicularian, Oikopleura dioica. Dev. Gene. Evol. 218, 69–79.
Galione, A., McDougal, A., Busa, W.B., Willmot, N., Gillot, I., Whitaker, M., 1993. Redundant mechanisms of calcium-induced calcium-release underlying calcium waves during fertilization of sea-urchin eggs. Science 261, 348–352, 80.
Gallo, A., Russo, G.L., Tosti, E., 2013. T-type Ca2+ current activity during oocyte growth and maturation in the ascidian Styela plicata. PLoS One 8.
Gilland, E., Miller, A.L., Karplus, E., Baker, R., Webb, S.E., 1999. Imaging of multicellular large-scale rhythmic calcium waves during zebrafish gastrulation. Proc. Natl. Acad. Sci. 96, 157–161.
Halbleib, J.M., Nelson, W.J., 2006. Cadherins in development: cell adhesion, sorting, and tissue morphogenesis. Genes Dev. 20, 3199–3214.
Jaffe, L.F., 1999. Organization of early development by calcium patterns. Bioessays 21, 657–667.

Jørgensen, N.R., Geist, S.T., Civitelli, R., Steinberg, T.H., 1997. ATP-and Gap Junction–dependent Intercellular Calcium Signaling in Osteoblastic Cells. J. Cell Biol. 139 (2), 497–506.
Kaneuchi, T., Sartain, C.V., Takeo, S., Horner, V.L., Buehner, N.A., Aigaki, T., Wolfner, M.F., 2015. Calcium waves occur as *Drosophila* oocytes activate. Proc. Natl. Acad. Sci. 112, 791–796.
Kari, W., Zeng, F., Zitzelsberger, L., Will, J., Rothbächer, U., 2016. Embryo microinjection and electroporation in the chordate *Ciona intestinalis*. J. Vis. Exp 1–10.
Kashir, J., Deguchi, R., Jones, C., Coward, K., Stricker, S.A., 2013. Comparative biology of sperm factors and fertilization-induced calcium signals across the animal kingdom. Mol. Reprod. Dev. 80, 787–815.
Kester, D.R., Duedall, I.W., Connors, D.N., Pytkowicz, R.M., 1967. Limnol. Oceanogr. 12, 176–179. Department of Zoology and Plankton Laboratory, University of Southampton, England.
Lacinova, L., 2011. T-type calcium channel blockers – new and notable. Gen. Physiol. Biophys. 30, 403–409.
Langley, A.R., Smith, J.C., Stemple, D.L., Harvey, S.A., 2014. New insights into the maternal to zygotic transition. Development 141, 3834–3841.
Lee, K.W., Webb, S.E., Miller, A.L., 1999. A wave of free cytosolic calcium traverses zebrafish eggs on activation. Dev. Biol. 214, 168–180.
Leuranguer, V., Mangoni, M.E., Nargeot, J., Richard, S., 2001. Inhibition of T-type and L-type calcium channels by mibefradil: physiologic and pharmacologic bases of cardiovascular effects. J. Cardiovasc. Pharmacol. 37, 649–661.
Levin, M., 2007. Gap junctional communication in morphogenesis. Prog. Biophys. Mol. Biol. 94, 477–479.
Martin, R.L., Lee, J.H., Cribbs, L.L., Perez-Reyes, E., Hanck, D.A., 2000. Mibefradil block of cloned T-type calcium channels. J. Pharmacol. Exp. Ther. 295, 302–308.
McDougall, A., Sardet, C., 1995. Function and characteristics of repetitive calcium waves associated with meiosis. Curr. Biol. 5, 318–328.
Miao, Y.-L., Stein, P., Jefferson, W.N., Padilla-Banks, E., Williams, C.J., 2012. Calcium influx-mediated signaling is required for complete mouse egg activation. Proc. Natl. Acad. Sci. 109, 4169–4174.
Mikhaleva, Y., Kreneisz, O., Olsen, L.C., Glover, J.C., Chourrout, D., 2015. Modification of the larval swimming behavior in Oikopleura dioica, a chordate with a miniaturized central nervous system by dsRNA injection into fertilized eggs. J. Exp. Zool. B Mol. Dev. Evol. 324.
Mikhaleva, Y., Skinnes, R., Sumic, S., Thompson, E.M., Chourrout, D., 2018. Development of the house secreting epithelium, a major innovation of tunicate larvaceans, involves multiple homeodomain transcription factors. Dev. Biol. 0–1.
Omotezako, T., Nishino, A., Onuma, T.A., Nishida, H., 2013. RNA interference in the appendicularian Oikopleura dioica reveals the function of the Brachyury gene. Dev. Gene. Evol. 223, 261–267.
Permenter, M.G., Lewis, J.A., Jackson, D.A., 2011. Exposure to nickel, chromium, or cadmium causes distinct changes in the gene expression patterns of a rat liver derived cell line. PLoS One 6.
Pfaffl, M.W., 2001. A new mathematical model for relative quantification in real-time RT-PCR. Nucleic Acids Res. 29, e45.
Robb-Gaspers, L.D., Thomas, A.P., 1995. Coordination of Ca2+ signaling by intercellular propagation of Ca2+ waves in the intact liver. J. Biol. Chem. 270 (14), 8102–8107.
Runft, L.L., Jaffe, L.A., Mehlmann, L.M., 2002. Egg activation at fertilization: where it all begins. Dev. Biol. 245, 237–254.
Ruta, L.L., Popa, V.C., Nicolau, I., Danet, A.F., Iordache, V., Neagoe, A.D., Farcasanu, I.C., 2014. Calcium signaling mediates the response to cadmium toxicity in Saccharomyces cerevisiae cells. FEBS Lett. 588, 3202–3212.
Samuel, A.D.T., Murthy, V.N., Hengartner, M.O., 2001. Calcium dynamics during fertilization in C. elegans. BMC Dev. Biol. 1, 1–6.
Sartain, C.V., Wolfner, M.F., 2013. Calcium and egg activation in Drosophila. Cell Calcium 53, 10–15.
Simoncini, L., Block, M.L., Moody, W.J., 1988. Lineage-specific development of calcium currents during embryogenesis. Science 242, 1572–1575, 80.
Søviknes, A.M., Glover, J.C., 2007. Spatiotemporal patterns of neurogenesis in the appendicularian Oikopleura dioica. Dev. Biol. 311, 264–275.
Speksnijder, J.E., Sardet, C., Jaffe, L.F., 1990. Periodic calcium waves cross ascidian eggs after fertilization. Dev. Biol. 142, 246–249.
Stach, T., Winter, J., Bouquet, J.M., Chourrout, D., Schnabel, R., 2008. Embryology of a planktonic tunicate reveals traces of sessility. Proc. Natl. Acad. Sci. U. S. A. 105, 7229–7234.
Stricker, S.A., 1996. Repetitive calcium waves induced by fertilization in the nemertean worm Cerebratulus lacteus. Dev. Biol. 176, 243–263.
Stricker, S.A., 1999. Comparative biology of calcium signaling during fertilization and egg activation in animals. Dev. Biol. 211, 157–176.
Tada, M., Concha, M.L., 2001. Vertebrate gastrulation: calcium waves orchestrate cell movements. Curr. Biol. 11, 470–472.
Tadros, W., Lipshitz, H.D., 2009. The maternal-to-zygotic transition: a play in two acts. Development 136, 3033–3042.
Verkhratsky, A., 2002. The endoplasmic reticulum and neuronal calcium signalling. Cell Calcium 32, 393–404.
Webb, S.E., Miller, A.L., 2003. Calcium signalling during embryonic development. Nat. Rev. Mol. Cell Biol. 4, 539–551.
Webb, S.E., Miller, A.L., 2006. Ca2+ signaling and early embryonic patterning during the Blastula and Gastrula Periods of Zebrafish and Xenopus development. Biochim. Biophys. Acta Mol. Cell Res. 1763, 1192–1208.
Webb, S.E., Miller, A.L., 2007. Ca2+ signalling and early embryonic patterning during zebrafish development. Clin. Exp. Pharmacol. Physiol. 34, 897–904.
Whitaker, M., 2006. Calcium at fertilization and in early development. Physiol. Rev. 86, 25–88.
Whitaker, M., 2008. Calcium signalling in early embryos. Philos. Trans. R. Soc. B Biol. Sci. 363, 1401–1418.
Wilding, M., Marino, M., Monfrecola, V., Dale, B., 2000. Meiosis-associated calcium waves in ascidian oocytes are correlated with the position of the male centrosome. Zygote 8, 285–293.
Xu, Z., Kopf, G.S., Schultz, R.M., 1994. Involvement of inositol 1,4,5-trisphosphate-mediated Ca2+ release in early and late events of mouse egg activation. Development 120, 1851–1859.
Yancey, S.B., Biswal, S., Revel, J.P., 1992. Spatial and temporal patterns of distribution of the gap junction protein connexin43 during mouse gastrulation and organogenesis. Development 114, 203–212.